ANNALS OF GEOPHYSICS, 68, 1, V107, 2025; doi:10.4401/ag-9155
OPEN ACCESS

Methana Magmatic Observational Experiment (MeMaX) – seismological monitoring of magmatic and tectonic activity in the western Saronic Gulf region, Greece

Jan-Phillip Föst[*,1,2], Joachim R. R. Ritter[2], Christos P. Evangelidis[3], Efthimios Sokos[4], Nicole Richter[1], Klaus R. Reicherter[1]

(1) RWTH Aachen University, Teaching and Research Area Neotectonics and Natural Hazards, Aachen, Germany
(2) Karlsruhe Institute of Technology, Geophysical Institute, Karlsruhe, Germany
(3) National Observatory of Athens, Institute of Geodynamics, Athens, Greece
(4) University of Patras, Laboratory of Seismology, Patras, Greece

Article history: received September 15, 2024; accepted December 16, 2024

Abstract

Large-scale historical volcanic eruptions caused significant destruction in the Mediterranean region (e.g., Thera/Santorini explosion circa 1600 BCE). The South Aegean Volcanic Arc remains active, and in addition to primary volcanic hazards such as ashfall and lava flows, active submarine and coastal volcanoes have the potential to trigger tsunamis as secondary volcanic hazard. These tsunamis pose a threat even to far-distant coastlines. With increasing population density, infrastructure development, and seasonal tourism, both primary and secondary volcanic risks along the Aegean coasts are increasing, even with respect to smaller, more frequent eruptions. Our focus is on the western Saronic Gulf region within the Aegean Sea, as possible impacts may even extend into the greater Athens metropolitan area. There, the dormant volcanoes of the Methana volcanic system, which last erupted in 230 BCE, and the submarine Pausanias Volcanic Field pose an underappreciated hazard. We search for evidence of yet undetected magmatic activity through the identification of related microseismic events and describe the design of the related MeMaX experiment. Since 2019, the National Observatory of Athens and the University of Patras operate six seismic stations on Methana and the nearby Peloponnese mainland. In March 2024, an additional 15 seismic recording stations were deployed for a two-years period across Methana, Aegina, Agistri, Kyra, and Poros islands and the mainland Peloponnese. This network configuration provides a dense and good azimuthal coverage of seismic ray paths for earthquake location and structural analysis. The continuous recordings enhance the observational capacities for earthquake detection, e.g. the first results indicate that the noise at the recording sites is quite low and that low magnitude events to *ML* ca. 0 can be recorded with a very good signal-to-noise ratio. This geophysical experiment is part of the MULTI-MAREX initiative.

Keywords: Seismic experiment; Volcano monitoring; Methana; Saronic Gulf; Greece

1. Introduction

Investigating dormant volcanoes such as the Methana and Pausanias volcanic complexes in Greece (Fig. 1) is of paramount importance, as these seemingly dormant systems can reawake to activity, posing significant risks to nearby infrastructure and communities. At present Methana and Pausanias are close-by complex magmatic systems with geodynamic and hydrothermal activity at the eastern coast of the Peloponnese (Fig. 1). They are the westernmost members of the South Aegean Volcanic Arc. The present time volcanic hazard of the Methana volcanic complex is considered to be low (Vougioukalakis and Fytikas, 2005). Despite that and its last eruption occurring around 230 BCE, ongoing thermal activity and gas emissions indicate that volcanism at Methana remains a potential hazard. The history of the eruptions on Methana and Pausanias (Pe-Piper and Piper, 2013; Foutrakis and Anastasakis, 2018a) and the general long-lived process of magma generation and the long residence time of several tens of thousands of years in lithospheric reservoirs (Rout et al., 2021) also indicate that future volcanic activity can be expected. Due to the proximity of Methana and Pausanias to Athens, with its vulnerable infrastructure and high population, it is known that even a low hazard potential can lead to a significant risk. Generally, low-magnitude volcanic eruptions can cause major impacts to our modern societies (Mani et al., 2021). Thus, understanding the seismic and magmatic activity as well as the associated volcanic hazards in and around Methana Peninsula is essential, particularly in the context of the complex tectonic dynamics of the area. This region, characterized by active fault systems and frequent seismic events, has been relatively under-investigated compared to other volcanic systems such as Santorini or Nisyros (Vougioukalakis and Fytikas, 2005). Especially, the influence of the current tectonic stress field on magmatic processes remains unknown.

Seismic monitoring of magmatic systems is an efficient tool to derive information concerning their in-situ physical state (e.g., Pallister and McNutt, 2015 and White and McCausland, 2019). In this respect, the Methana Magmatic Observational Experiment (MeMaX) addresses gaps in knowledge by deploying a dense temporary seismic network to densify observations between permanent stations. This approach allows to very sensitively monitor the microseismicity in the area. The goal of MeMaX is to detect previously undetected seismic events linked to both magmatic and tectonic processes, providing crucial insights into the region's geodynamic behavior including inner architecture and the tectonic stress field.

2. Regional setting

The Mediterranean Sea, a remnant of the ancient Tethys Ocean, presents a complex tectonic setting shaped by the interactions between the Eurasian, African, and Arabian plates, along with several microplates (Papanikolaou, 2021). The eastern Mediterranean, the oldest segment, retains remnants of the Tethys Ocean, while the western Mediterranean emerged from the opening of a post-collision basin following the Tethys's closure during the Cenozoic era (Papanikolaou, 2021). This regional tectonic framework is notably intricate due to the varied movements of the Anatolian, Aegean, Apulia-Adriatic, and Sinai microplates. The Anatolian microplate, moving westward at approximately 20 mm/year, is bounded by the Hellenic and Cyprus Arcs to the south, and by the North and East Anatolian Faults to the north and east. These active faults contribute to significant seismic activity, as found by the recent devastating earthquakes in Türkiye and Syria (Kusky et al., 2023). In contrast, the Aegean microplate moves at a faster rate of 40-50 mm/year (Clarke et al., 1998; McClusky et al., 2000) towards the southwest, driven largely by the subduction of the African plate beneath it. This subduction is also the driving mechanism for the formation of the Hellenic arc, a region marked by significant volcanic and seismic activity, particularly in the southern Hellenides (Papanikolaou, 2021).

The Aegean Sea (Fig. 1) is a tectonically active region framed by the Greek mainland and the Peloponnese peninsula to the north and west, Türkiye to the east, and the subduction zone between the African/Arabian and Eurasian plates to the south (Fig. 1). This region is notable for its significant volcanic and seismic activity, which has evolved in response to the complex tectonic processes. The volcanic history of the Aegean Sea can be divided into two main phases. The first phase began during the Oligocene and affected northern Greece, northwest Türkiye, and southern Bulgaria (Fytikas et al., 1984). After a pause in the middle Miocene, volcanic activity resumed in the southern Aegean during the late Pliocene, shifting to the South Aegean Volcanic Arc (Fytikas et al., 1984). This arc, which extends from the Saronic Gulf in western Greece to islands near the Turkish coast, includes volcanic centers such as Methana, Aegina, Poros, Milos, Santorini, and Nisyros. The shift in volcanic activity from north to south is

linked to changes in subduction dynamics and the formation of a back-arc region due to the rollback of the African plate, leading to crustal thinning in the southern Aegean (Papazachos and Comninakis, 1971; Fytikas et al., 1984; Dietrich et al., 1988; Pe-Piper and Piper, 2005; Papageorgiou, 2010; Jolivet et al., 2013). The South Aegean Volcanic Arc is characterized by calc-alkaline rocks associations typical of back-arc volcanism (Fytikas et al., 1984; Pe-Piper and Piper, 2005). The arc can be subdivided into western and eastern segments based on volcanic characteristics. The western segment, which includes Methana, Aegina, Poros and Milos, features volcanic domes and lava flows primarily composed of andesites and dacites (Fytikas et al., 1984; Pe-Piper and Piper, 2005) controlled by regional tectonics (Tzanis et al., 2018). In contrast, the eastern segment around Santorini and Nisyros is marked by volcanic cones and calderas, a result of more intense crustal deformation and thinning, caused by the geometry of the subduction zone (Fytikas et al., 1984; Le Pichon et al., 1997; Pe-Piper and Piper, 2002, 2005). The Saronic Gulf (Fig. 1), a western extension of the Aegean Sea, is a combination of different neotectonic basins shaped by the extensional tectonics of the back-arc region (Papazachos and Comninakis, 1971; Jolivet et al., 2013). This gulf is divided into western and eastern parts by a shallow N-S striking submarine platform extending from Salamis to Methana (Makris, 2004; Drakatos et al., 2005; Foutrakis and Anastasakis, 2020). The western part is more volcanically and seismically active (Fig. 2), with complex underground deformation, including the formation of graben and horst structures (Le Pichon and Angelier, 1979; Makris, 2004; Nomikou et al., 2013; Kolaiti and Mourtzas, 2016). Notable features include the Megara and Epidaurus basins, separated by the Korfos fault valley, an extension of the northwestern Corinthiakos Gulf fault zone (Papageorgiou, 2010; Foutrakis and Anastasakis, 2020). Different studies indicate a rotation of the tectonic stress field, from W-E in the Corinthiakos Gulf to WNW-ESE in the Saronic Gulf (Papanikolaou et al., 1988; Tzanis et al., 2018). According to Suckale et al. (2009) and Sachpazi et al. (2016), the Mohorovičić (Moho) discontinuity is at 30 km depth beneath the western Saronic Gulf. The deepest sea in the Saronic Gulf can be found in the Epidaurus basin with 421 meters depth (Foutrakis and Anastasakis, 2020).

2.1 Methana and its volcanism

The Methana Peninsula, covering an area of approximately 44 km², is the second westernmost volcanic system of the South Aegean Volcanic Arc (D'Alessandro et al., 2008). Its current state is dormant, but there is magmatic degassing and hydrothermal activity. There are more than 30 individual Quaternary volcanic domes (Antoniou et al., 2018) and the highest peak, Helona Mountain, rises to around 740 meters above sea level (Gatsios et al., 2020b) and it is one of the oldest volcanoes. There are active fumaroles (Fig. 1) near Nea Loutra (NL), Agios Nikolaos (AN), and hydrothermal activity at Thiafi Bay (TB, Fig. 1) (D'Alessandro et al., 2008) associated with faulting (Dotsika et al., 2010). The Methana Peninsula is situated within the extensional tectonic setting of the Saronic Gulf, where the continental crust is estimated to be relatively thin (20-30 km thickness)(Karagianni et al., 2004; Drakatos et al., 2005; Papazachos, 2019). The extensional forces in this region led to the development of a complex fault network (Fig. 2), including older NW-SE and NNE-SSW faults and younger E-W striking faults (Nomikou et al., 2013; Gatsios et al., 2020b). These faults not only delineate the peninsula but also can facilitate magma ascent, thus contributing to the volcanic activity (D'Alessandro et al., 2008).

The basement of Methana is composed of Jurassic to Cretaceous limestones, which are exposed in the southern and northwestern parts of the peninsula (Pe-Piper and Piper, 2013). The volcanic history of Methana likely began around 1.5 Myrs ago, although some studies suggest that it may have started as early as the late Pliocene (Dietrich et al., 1988; Nomikou et al., 2013; Pe-Piper and Piper, 2013). The volcanic activity on Methana has predominantly been effusive (only about 14 eruptions), characterized by low eruption rates and limited spatial extent (Schoenhofen et al., 2020). However, some evidence of smaller explosive events (about 3) exists, indicated by layers of tuff found at various outcrops (Pe-Piper and Piper, 2013). Chemical analyses of the volcanic deposits suggest that the melt originated from a mix of mantle and crustal material, with a greater crustal influence compared to other Aegean volcanic systems like Santorini and Nisyros (Elburg et al., 2018; Woelki et al., 2018). According to Tzanis et al. (2020) Methana is directly located above the rapidly subducting segment of the Hellenic Subduction System. Focal plane mechanisms and hypocenters of subcrustal earthquakes (Hatzfeld et al., 1989), see also Fig. 3 and tomographic imaging (Sachpazi et al., 2016) indicate an inflection of the slab in a depth of 50-60 km under the Argolic Gulf southwest of Methana.

Earthquake activity indicates that the slab is likely at 100 km depth underneath Methana (Fig. 3). At this depth and its related lithostatic pressure, the eclogite facies metamorphism drives water into the mantle wedge and

initiates the generation of andesitic magmas and arc volcanism (Grove et al., 2006; Tzanis et al., 2018). The volcanic evolution of Methana can be divided into eight distinct phases, each reflecting changes in tectonic activity and volcanic processes over time. According to Pe-Piper and Piper, (2013), the activity started at first with andesitic and dacitic domes forming along the dominating N-S striking fault system. These domes eroded and were subjected to uplift and additional faulting. Basaltic-andesitic eruptions continued and covered mostly the northern part of the peninsula. About 0.9-0.5 Myrs ago the tectonic framework started to evolve to a more E-W striking normal fault system. Around 0.34-0.29 Myrs ago pyroclastic explosive eruptions and multiple effusive eruptions occurred. The most recent volcanic event on Methana near the village Kameni Chora occurred in 230 BCE at Kameno Vouno volcano, resulting in the formation of the prominent Mavri Petra lava flow in the northwest of the peninsula.

Underneath Kameno Vouno and the Pausanias volcanic field, Tzanis et al. (2020) found an increased magnetic susceptibility domain that reaches down to 2 km depth using magnetotelluric measurements. This is interpreted as igneous rocks with intermediate to mafic compositions. Underneath the eastern and central domes, a similar magnetic susceptibility domain reaches down to ca. 4 km depth. Studies of long stacked Sentinel-1 C-band Synthetic Aperture Radar (SAR) images acquired from March 2015 to August 2019 in combination with Global

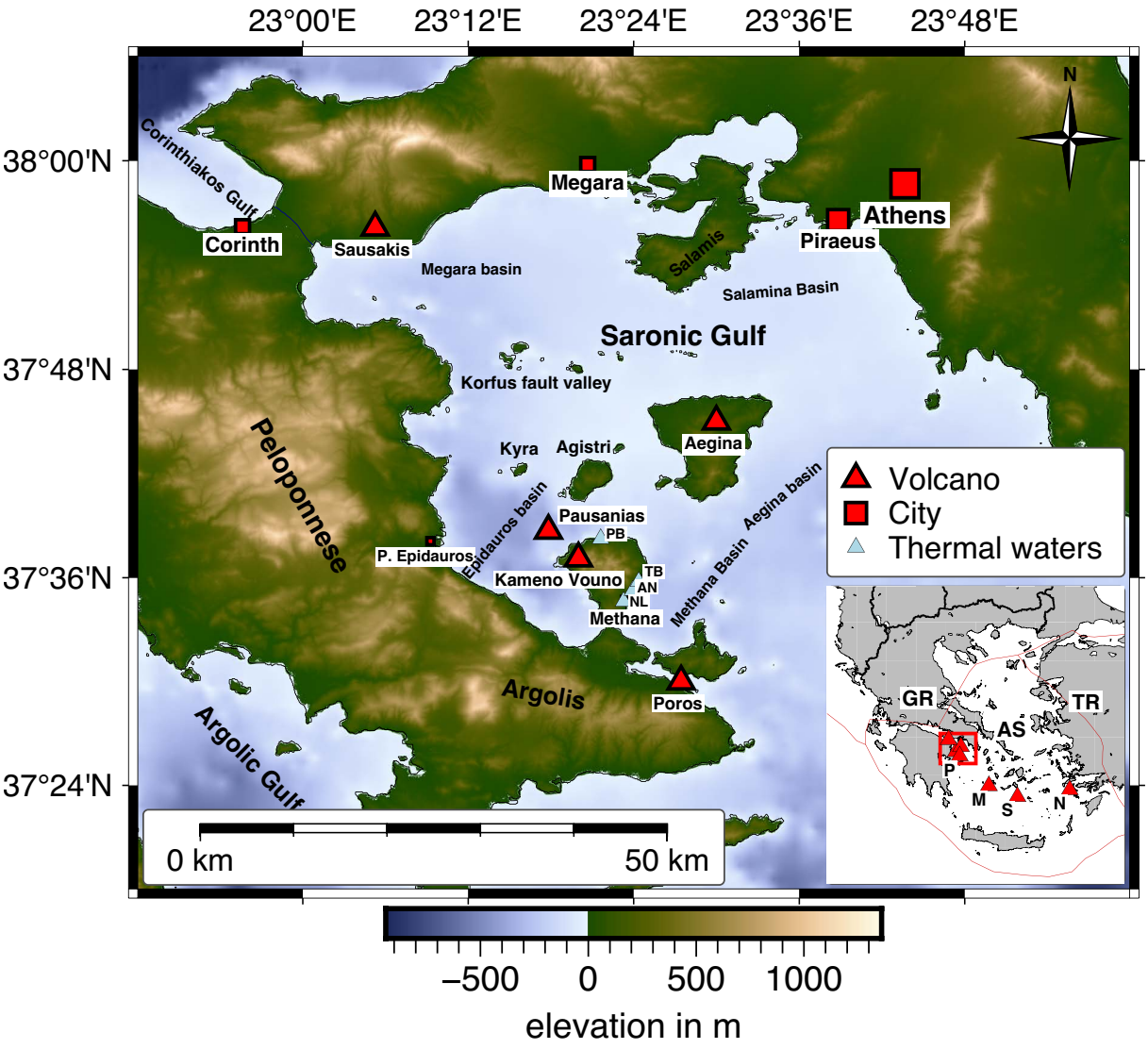

Figure 1. Overview of the Saronic Gulf and the research area. For orientation, the cities of Athens, Corinth, Megara, P. Epidauros, and Piraeus are marked with rectangles, as well as the volcanoes and basins in the region. Marked with blue triangles are thermal waters around Methana: Agios Nikolaos (AN), Nea Loutra (NL), Pausanias Baths (PB), and hydrothermal activity at Thiafi Bay (TB). In the overview in the bottom right corner, the South Aegean Volcanic Arc is marked with its volcanic systems from west to east starting in the Saronic Gulf: Poros (P), Milos (M), Santorini (S), and Nisyros (N). The Aegean Sea (AS) is also marked. The red lines indicate the plate boundaries.

Navigation Satellite System (GNSS) stations resulted in line of sight displacement velocities of −18.1 mm/year to +7.5 mm/year on Methana peninsula. These deformations are interpreted as near-surface effects. They do not seem to be related to magmatic inflation or deflation, which is consistent with the current low magmatic activity at Methana (Gatsios et al., 2020a).

2.2 Submarine Pausanias Volcanic Field

The submarine Pausanias Volcanic Field is located just to the northwest of the Methana Peninsula and spans approximately 36 km² plus wide-spread volcaniclastic deposits (Foutrakis and Anastasakis, 2018a,b). It is composed of at least six cone-like volcanic centers which are active during three periods. The first volcanic period began at around 450 ka, correlating with the Methana volcanic history. The second and most significant event occurred between 200 ka and 130 ka, expanding the volcanic field towards north and west. The youngest volcanic series occurred at ca. 14 ka. The volcanic field is bounded on the east by a shallow submarine platform that delineates the western and eastern parts of the Saronic Gulf. The eastern flank of the volcanic field reaches the seafloor at around 270 meters depth, while its western flank extends down to the adjacent Epidaurus basin at depths ranging from

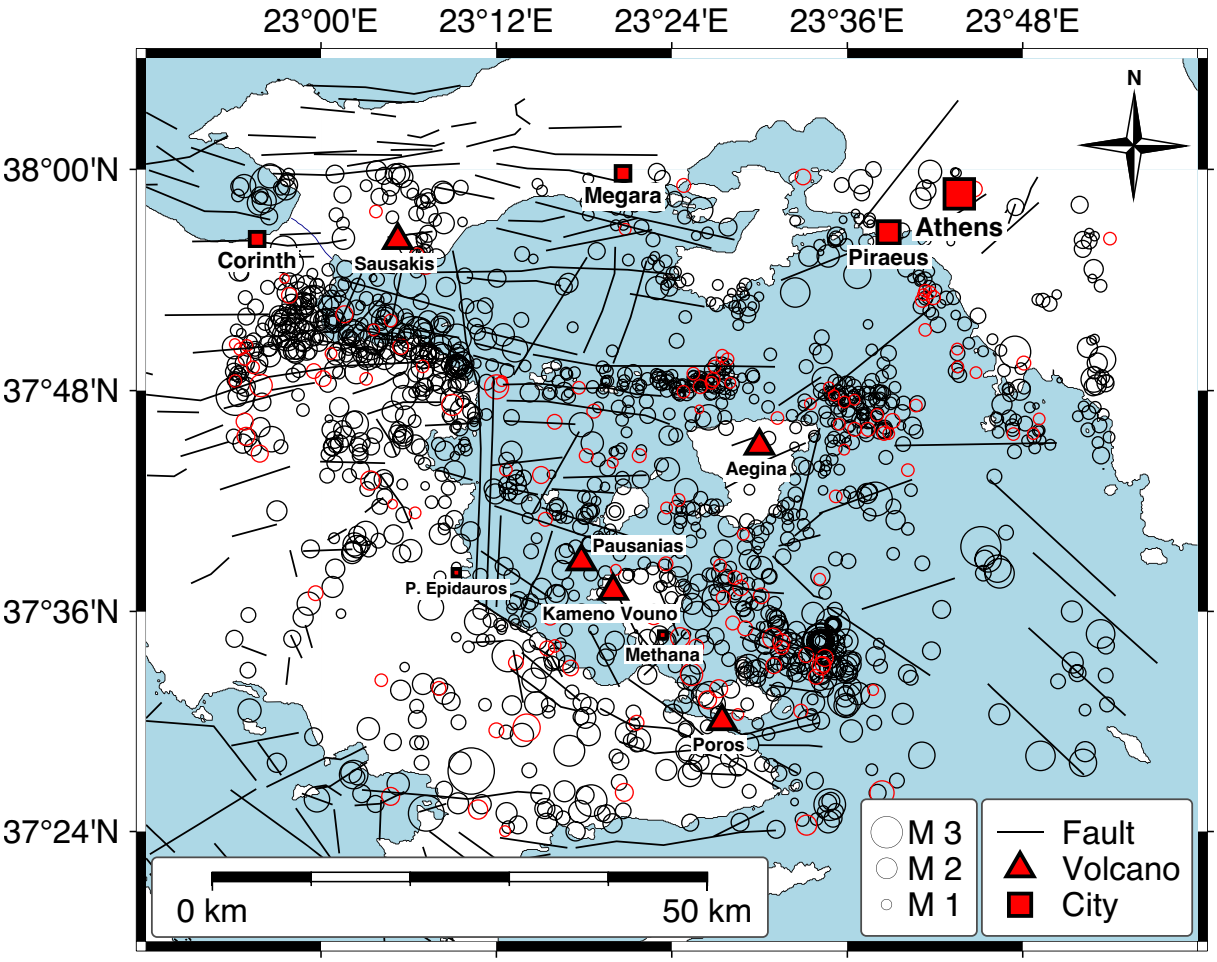

Figure 2. Overview of the seismic activity detected by the National Observatory in Athens (2019-2024) in the Saronic Gulf and the research area. These locations include data from the permanent stations on Methana (networks HL, HA), starting in 2019, up to 8 September 2024, indicated as circles. Events that occurred since the deployment of the network 1A (27 March 2024) are marked with red circles. For orientation, the cities of Athens, Corinth, Megara, Methana, Piraeus, and P. Epidauros are marked with rectangles, as well as the volcanoes in the region with red triangles. Black lines indicate main faults collected from (Stefatos et al., 2002; Skourtsos and Kranis, 2009; Foutrakis and Anastasakis, 2020; Tzanis et al., 2020).

380 m to 421 m. The seafloor is composed of Mesozoic limestone. The highest summit of the volcanic field rises to a depth of 143 m below sea level (Nomikou et al., 2013). The Pausanias Volcanic Field primarily consists of dacitic material, suggesting a connection with or similar melt generation as the volcanic processes that occurred on the Methana Peninsula (Foutrakis and Anastasakis, 2018a,b).

3. Network Description

The network Methana Magmatic Observational Experiment (MeMaX) is composed of permanent and temporary seismic stations which are included in the European Integrated Data Archive (EIDA). The stations of the National Observatory of Athens Seismic Network run under network code HL (National Observatory of Athens, Institute of Geodynamics, Athens, 1975), the Hellenic Seismological Network from the University of Athens under HA (University of Athens, 2008) and the network code for the temporary stations is 1A (Föst et al., 2024). Network 1A comprises 15 short-period seismic stations distributed across the Methana Peninsula, Aegina, Agistri, Kyra, and Poros islands,

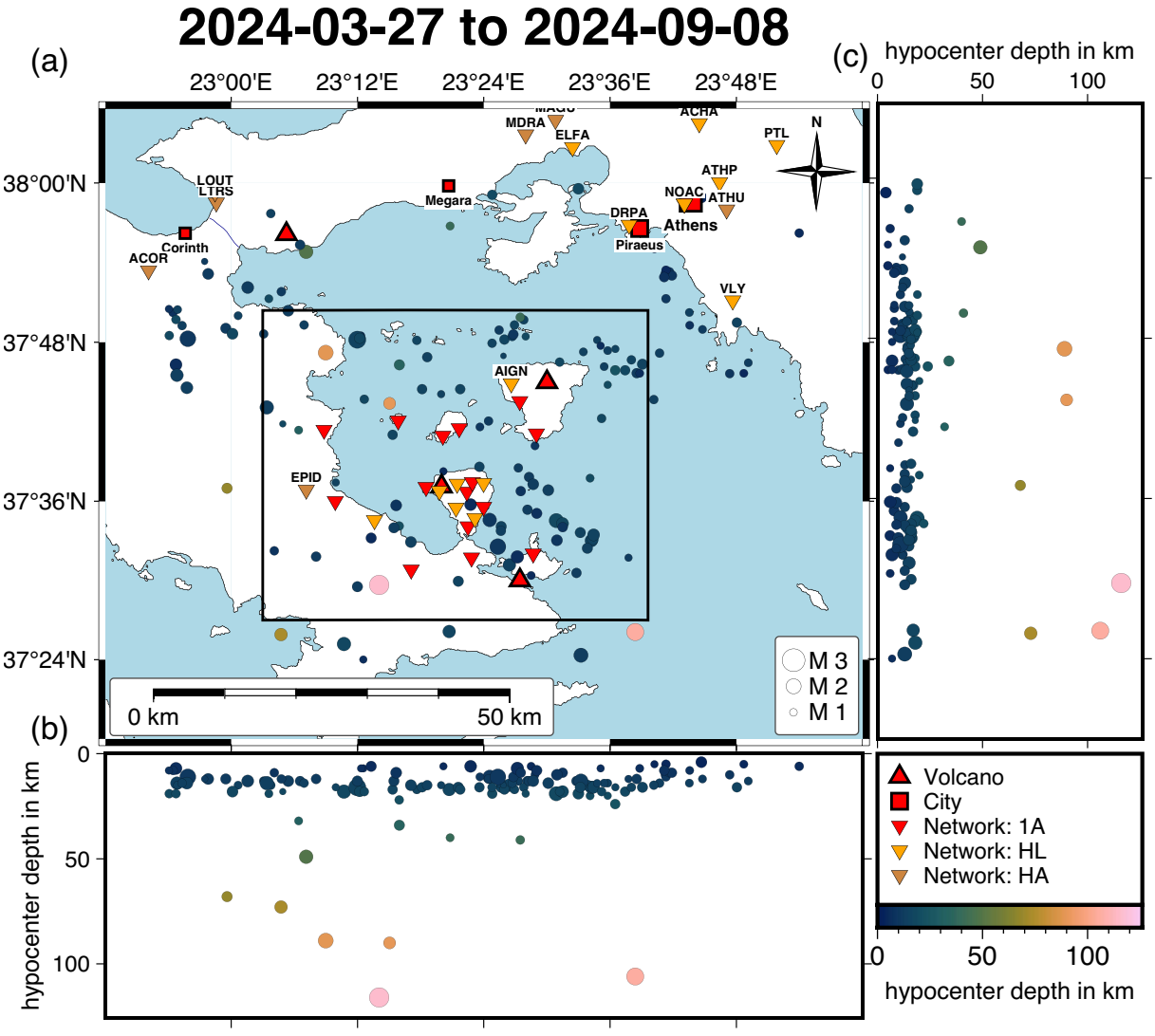

Figure 3. The MeMaX experiment includes all available seismic recording stations from the networks HL, HA, and 1A (see Data and Resources). The hypocenters outline the ongoing seismic activity detected by the National Observatory in Athens since the deployment of the MeMaX network (27 March 2024) until 8 September 2024, (b) longitudinal depth slice, and (c) latitudinal depth slice. For orientation, the hypocenter depth is indicated with color. Additionally, the cities of Athens, Corinth, Megara, and Piraeus are marked with rectangles, as well as the volcanoes in the region with red triangles. The main study area is indicated with the black frame (see Fig. 5).

and the mainland of the Peloponnese (Figs. 3 and 5). The temporary installation began with the setup of 14 stations between March 13th and 29th, 2024, in the Methana area, and was completed with the 15th station on Kyra Island on June 10th, 2024. Recording is planned to continue for a two-year period.

3.1 Instrumentation

The permanent stations of network HL consist of four short-period stations which were installed at Ano Fanari (MET3), Agious Theodorous (MET4), Makriloggos (MET5) and Megalochori (MET6) on Methana peninsula starting in February 2019. These are equipped with EarthData recorders and Lennartz LE-3D 1 s seismometers. The vaults for two broadband seismic stations were constructed at Methana town (MET1) and Kameni Chora (MET2) and these stations are equipped with Güralp CMG3-ESPC 100 s seismometers and Güralp Minimus and Reftek-130 recorders, respectively. A permanent co-located GNSS station is operating at MET2 since 2019 and a co-located strong motion sensor is operating at MET1.

All temporary 1A stations are equipped with MARK L-4C-3D seismometers, which have a flat ground velocity response ranging from the corner frequency of 1 Hz to more than 100 Hz. These are passive systems designed for low power consumption, making them suitable for remote stations. Data is logged using DiGOS DATA-CUBE^3 recorders with 32 GB SD drives, operating at a sampling rate of 100 samples per second and ca. 0.13 W power consumption. Both instruments are borrowed from the Geophysical Instrument Pool Potsdam (GIPP).

To ensure continuous power supply, all temporary stations are connected to 12 V batteries charged daily by 20 W_{peak} solar panels. Solar chargers prevent battery damage. To protect the equipment, the batteries, data loggers, and solar chargers are housed in water-resistant bags and packed inside boxes, which can release water at the bottom to prevent flooding during possible heavy rains (Fig. 4d). The seismometer and the equipment box are buried next to each in separate holes at ca. 30 cm depth (Fig. 4e). Firm coupling of the seismometers to the ground is enhanced by a foundation made of approximately 5-8 cm of quick-setting cement (Fig. 4a). For mechanical protection and thermal insulation, the seismometers are packed into bags and wrapped in fleece material (Fig. 4c).

Seismometers were oriented to true north using a gyroscope (iXBlue Quadrans). Stations MM07 and MM11 were oriented using a traditional magnetic compass and a mobile phone compass. The precise horizontal orientation allows for e.g. accurate wave polarization analyses for receiver function or shear wave splitting methods. A high-quality time signal was established via the global positioning system (GPS) time synchronization, with the GPS antenna mounted on top of a wooden post (Fig. 4f). Reception of the GPS signal and time synchronization is done in a cycled mode, meaning that only every 30 minutes the internal clock synchronized to save power.

To ensure optimal sun exposure, the solar panels are mounted on top of the buried boxes or close-by rocks, oriented to about south sun and angled at approximately 45 degrees to facilitate the removal of dust and dirt by rainfall. Due to the remote sites, each station is marked with a warning sign (Fig. 4f) displaying contact information to deter curious hikers from digging.

3.2 Location Selection

To achieve the research objectives, all temporary station locations were strategically selected to fill observational gaps in the existing permanent network, which comprises stations from the National Observatory of Athens Seismic Network (HL) and the Hellenic Seismological Network (HA) (Fig. 3). The primary goal of the network design was to reduce the distance between seismic stations and achieve a comprehensive coverage of the research area. Especially recording stations were installed on the islands of the Saronic Gulf to increase the observational capabilities. On Methana Peninsula, we aimed to establish a very dense network across the entire peninsula to be able to record low-magnitude magmatic events ($ML \approx 0$). This led to the deployment of five additional stations, and thus in total 10 stations were running on Methana.

For the broader Saronic Gulf area and to ensure a better ray coverage throughout the region, we deployed four stations on the Peloponnese Peninsula and six stations on the surrounding islands – one on Poros, two on Agistri, two on Aegina and one on Kyra Island – in this way we achieved a large enough network encircling Methana and the submarine Pausanias Volcanic Fields. This strategic placement of stations is expected to enhance the accuracy of earthquake locations, both in depth and horizontally.

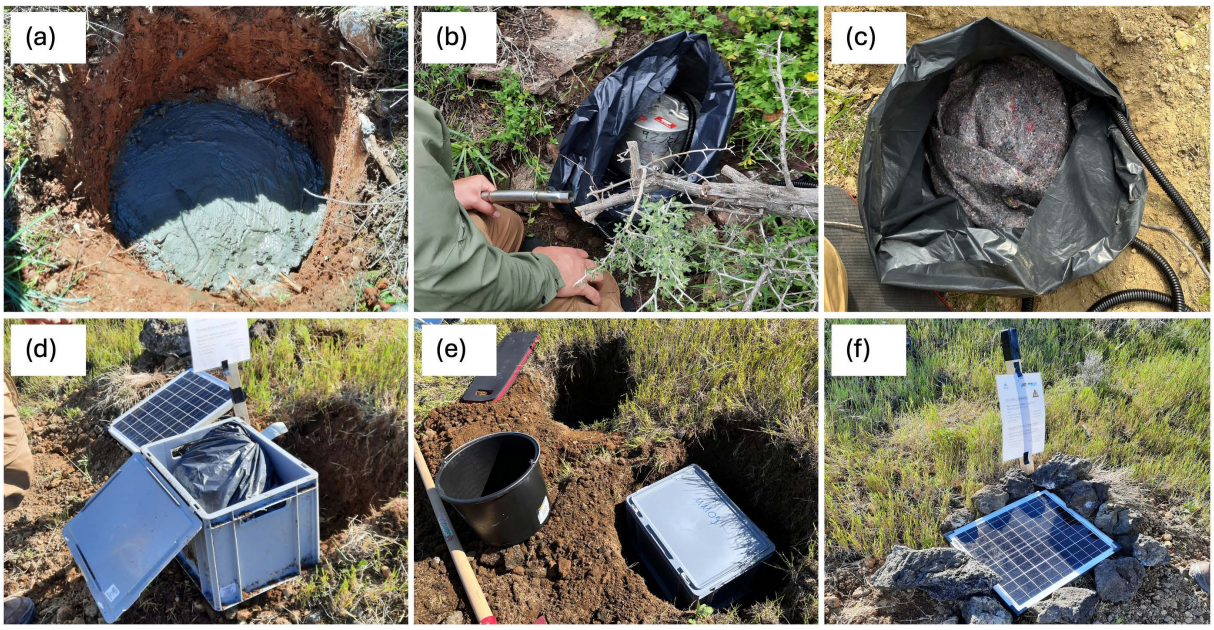

Figure 4. Installation of instruments of the 1A network in spring 2024: (a) Foundation for better surface coupling, (b) seismometer packed into bags, (c) thermal insulation, (d) equipment box, (e) two separated holes for equipment and seismometer, (f) final appearance of station MM09 with solar panel and warning sign at the GPS post.

The combined permanent and temporary networks enable us to determine a new seismic velocity model of the region in both 1-D, using VELEST (Kissling et al., 1994; Kissling et al., 1995), and 3-D, using SIMULPS14 (Thurber, 1983; Eberhart-Phillips and Michael, 1993; Haslinger and Kissling, 2001). Additionally, they help address unresolved issues, such as determining the Moho depth through the analysis of teleseismic receiver functions. The dense network on Methana is particularly aimed at detecting previously undetected magmatic microseismicity, similar to findings in the Eifel region (Hensch et al., 2019; Ritter et al., 2024). Magmatic earthquakes could indicate ongoing magmatic activity beneath Methana or Pausanias (see more in Section Data Quality) and can be distinguished from tectonic earthquakes based on their depth, characteristic waveform signatures, frequency content, and spatial clustering near volcanic structures. This network will also improve the precision of tectonic earthquake locations and thereby enhance the detection of active fault structures in the region, including fault plane solutions to resolve the stress field.

3.3 Network Operation

The temporary network 1A operates offline, without real-time data acquisition due to financial limitations and the need to minimize power consumption. The dataloggers use 32 GB SD cards to store the recorded data, which is collected during two service visits per year. The data is then archived at GFZ and GEOFON (Föst et al., 2024).

Data processing and analysis are conducted after merging the available data from the three networks. Polarity and amplitudes are carefully checked to ensure the correct use of metadata across all networks (see below). The public release of the archive for the 1A network is planned for the end of 2026 (see Data and Resources). As seen in Fig. 3 since the deployment of the network, NOA has detected more than 100 seismic events in the study area. For the planned recording period this should result in about 500-600 detected events using standard methods. This number should be increased by the use of all stations for detections and improved AI detection methods using SeisBench (Münchmeyer et al., 2022; Woollam et al., 2022) or Phase Neural Operator for Multi-Station Picking (Sun et al., 2023).

4. Data Quality

Our primary goal is to investigate hitherto undetected microseismicity in the study region (Fig. 5). Therefore, the background noise – and consequently the detection threshold – must be as low as possible at the remote recording

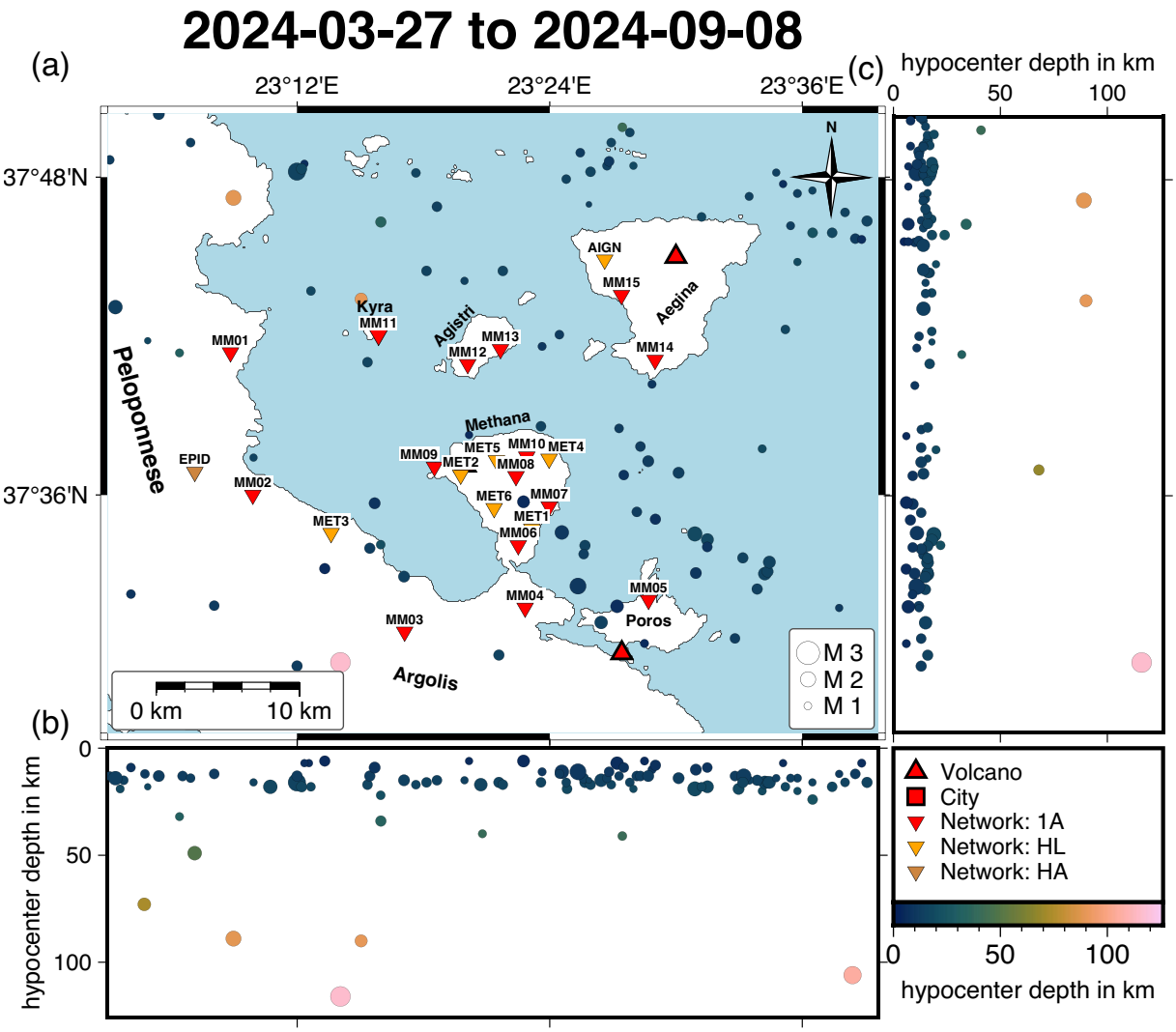

Figure 5. Detailed map of the main study area, including all available seismic recording stations with station codes from the networks HL, HA, and 1A (see Data and Resources). The hypocenters outline the ongoing seismic activity detected by the National Observatory in Athens since the deployment of the MeMaX network (27 March 2024) until 8 September 2024, (b) longitudinal depth slice, and (c) latitudinal depth slice. For orientation, the hypocenter depth is indicated with color. Additionally, the islands of Aegina, Agistri, Poros, and Kyra as well as the peninsula Methana are marked. The volcanoes in the region are indicated with red triangles.

stations in the main frequency range of interest which is ca. 1-20 Hz. Low noise levels are essential for investigating phenomena such as deep low-frequency (DLF) events within the plumbing systems of the Methana and Pausanias magmatic systems. Ideally, we aim to detect earthquakes like DLFs occurring possibly in the upper mantle with low magnitudes and hypocentral distances of approximately 50 km (e.g., 40 km depth and 30 km epicentral distance). Such geometries are known from other magmatic and tectonic systems: Eifel Volcanic Fields (Hensch et al., 2019), Hawaii (Aki and Koyanagi, 1981), or Central Africa (Batte et al., 2021). According to Ritter et al. (2024), particle velocity power spectral density (PSD_{vel}) values of around −180 dB to −185 dB (relative to 1 $m^2/(s^2\ Hz)$) would be sufficient for the network sites to detect DLF events of $ML = 0$ with frequencies between 1 Hz and 9 Hz. Tectonic earthquakes with magnitudes around 0 to −1 occur at frequencies around 15-20 Hz (Aki and Richards, 1980).

To assess the noise levels at each station, we calculated probabilistic power spectral densities (PPSD) using ObsPy (Beyreuther et al., 2010), as shown in Fig. 6. The analyzed time windows from 26 March to 5 June 2024 corresponds to the start of the temporary network 1A until the first collection of the field data. For reference, we also include the new high and low noise models (NHNM, NLNM) as defined by Peterson (1993).

All MeMaX stations have average noise levels below the NHNM with the exception of MET3 where a technical problem occurred. In the frequency interval of interest, 1-20 Hz, the noise levels are mostly below −160 dB, a few

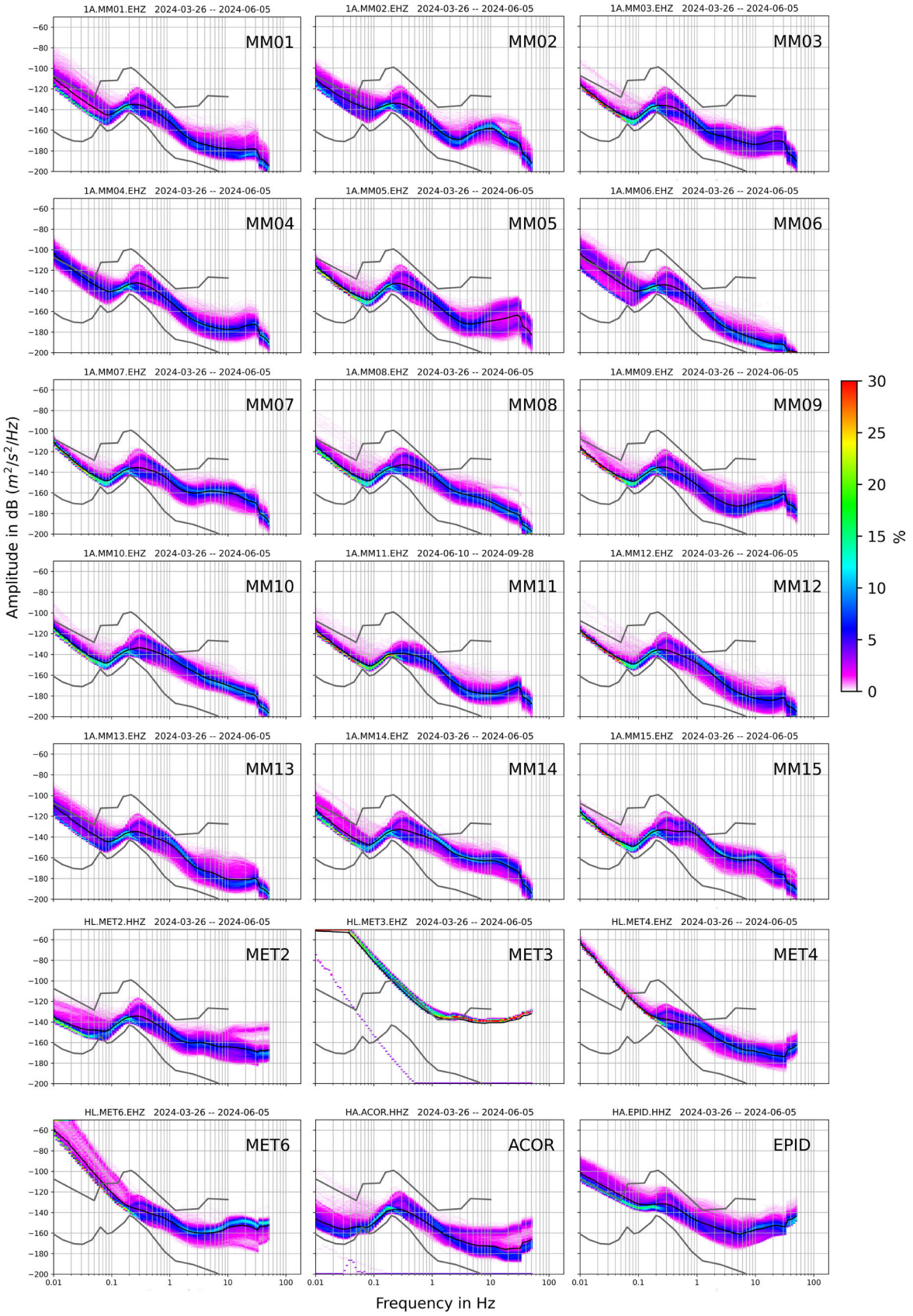

Figure 6. PPSDs for the recording time 26 March-5 June 2024 (until the first service for all stations in the area of MeMaX). The results for the vertical component recordings are presented (for horizontal components, see Figs. A1 and A2). The PPSDs are calculated for one-hour time windows with an overlap of 50 %. The colour coding represents the probability of a spectral power density to occur at a certain frequency. The grey lines show the new high and low noise models (NHNM, NLNM) after Peterson, (1993). The black line indicates the median noise level.

are below 180 dB. Below a frequency of 1 Hz, at ca. 0.2-0.4 Hz there is the second microseism peak due to oceanic waves. This peak is even clearly found at the short-period (1-100 Hz) instruments which seem to record well to frequencies as low as ca. 0.1 Hz. This allows to record teleseismic P- and S-waves for travel time, receiver function and shear splitting studies. At stations MM02, MM05, and MET6 there is an additional peak at around 10 Hz, likely due to anthropogenic noise. The increase in amplitude observed at frequencies below 0.2 Hz at stations MET4 and MET6 is a result of the instrument's limitations. These frequencies fall outside the range of the instrument's transfer function, leading to a distortion where the signal is effectively attenuated.

In Fig. 7 the median PPSD levels are presented for all stations of the MeMaX experiment. In the frequency range of interest, the noise levels range between −140 dB and −190 dB (MET3 seems to suffer from a technical problem). Station MM06 has the lowest noise level on Methana Peninsula with −155 dB to −190 dB for frequencies between 1 Hz and 10 Hz. Stations MM12 and MM13, both installed on Agistri Island, also exhibit low noise levels of −150 dB to −180 dB for this frequency range. The highest noise levels are found at stations MM14 and MM15 between −140 dB to −160 dB, which are both located on Aegina Island. Although the sites of MM14 and MM15 are some hundred meters away from some homes, this may be related with the manifold tourism on the island. Stations MM02 and MM07 are also associated with higher noise levels (around −160 dB) due to their proximity to agricultural activities.

The MARK L-4 seismometers installed at the temporary sites are short-period instruments with a nominal lower frequency corner of the response function at 1 Hz. The PPSD plots indicate that a reasonable ground motion can be recorded to ca. 0.1 Hz (Figs. 6 and 7). For a lower frequency range ($f < 0.1$ Hz), only the Nanometrics Trillium Horizon with a natural period of 120 s at station ACOR does reliably record the ground motion (Fig. 6). In comparison to the permanent HL and HA networks (Evangelidis et al., 2021), the noise levels of the temporary station sites are comparably good between 1 Hz and 20 Hz. This can be explained with the more flexible criteria for locations, because of an autonomous power supply, no requirement for the availability of data transmission and just short-term occupation of land.

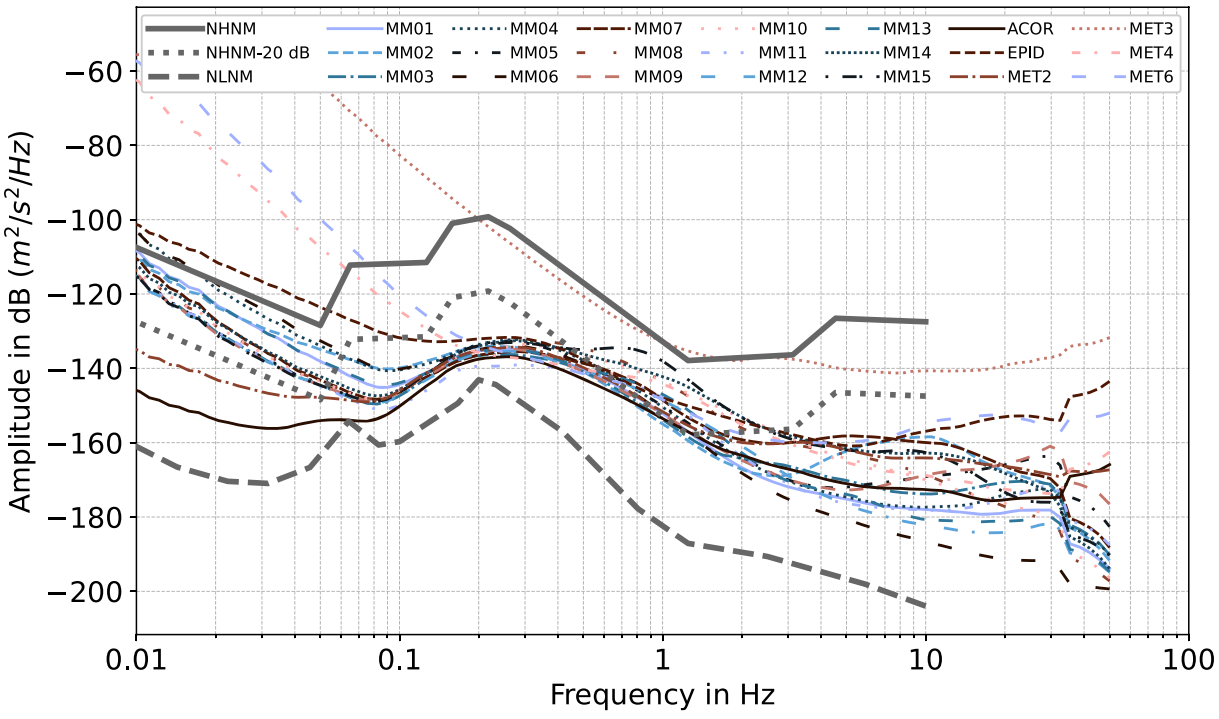

Figure 7. Median PPSD levels of for all stations in the MeMaX network. The gray lines show the new high and low noise models (NHNM, NLNM) as proposed by Peterson (1993) as well as the 20 dB reduced NHNM.

To check the wave polarity and correct individual removal of the instrument response, we compare the first onsets of three teleseismic earthquakes at all stations (see Fig. 8). Due to the long epicentral distances of more than 9,000 km and the relatively short aperture of the network, the seismic waves travel along very similar propagation

paths. Thus, the recorded waveforms should be very coherent at all MeMaX stations, except for local site effects such as variations in sediment thickness or seismometer coupling to the ground. The waveform comparison demonstrates the expected coherency. Also, the wave polarities are the same at the different stations. Interestingly, the short-period instruments show clear seismic phases below 0.1 Hz (Fig. 8). This is only possible, because the noise at the sites is quite low so that the signals are visible even more than four octaves below the lower corner frequency of the response function (Scherbaum, 2001). Of course, the amplitudes are lower than for the true ground motion, and a part of the low frequency content is missing, however, this can be corrected with a simulation filter (Scherbaum, 2001) at a later stage.

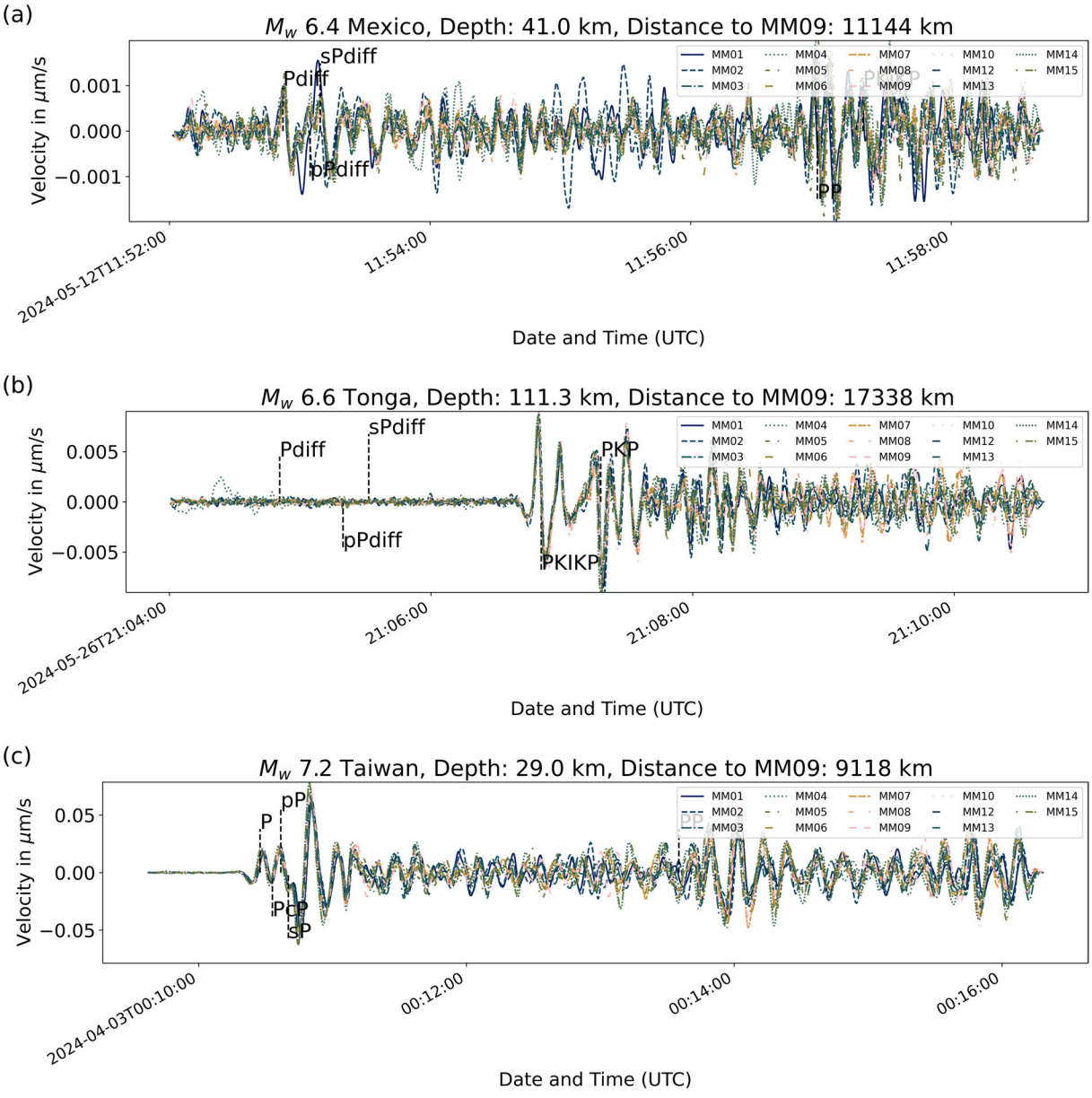

Figure 8. Waveform recordings for three teleseismic earthquakes are presented, showing the vertical channels for all stations (for horizontal channels see Figs. A3 and A4). The response function is removed to show the actual recording even at very low frequencies (<0.1 Hz), see text. (a) The first arrivals of the *Mw* 6.4 earthquake on 12 June 2024, in Mexico at a depth of 41 km. (b) The first arrival of the *Mw* 6.6 earthquake on 26 June 2024, in Tonga at a depth of 111.3 km. (c) The first arrival of the *Mw* 7.2 earthquake on 3 April 2024, in Taiwan at a depth of 29 km. The recordings are bandpass filtered with a lower cutoff frequency of 0.01 Hz and an upper cutoff frequency of 0.1 Hz. Linear trends and the mean are subtracted. The theoretical arrival phases are indicated, calculated using TauPy in ObsPy with the ak135 Earth model (Kennett et al., 1995).

At a distance of 11,144 km to station MM09, the first arrival Pdiff phase is clearly visible from a moderately strong earthquake (*Mw* 6.4) below Mexico (Fig. 8a). The following PP phase and PKIKP phase are also recorded with a good signal-to-noise ratio (SNR). The average noise level during daytime (ca. 15:00 local time and between 0.01 Hz to 0.1 Hz) is around ±0.5 nm/s, see traces in Fig. 8a. In Fig. 8b core phases from a deep Tonga event (*Mw* 6.6) are well recorded. Such phases together with array processing of the MeMaX recordings may be used for studying structures in the lower mantle or core for ray paths so far not covered. The P and PcP phases (Fig. 8c) of a Taiwan earthquake (*Mw* 7.2) can be used for teleseismic tomography or receiver function studies.

To test the capability of the MeMaX network in detecting regional low-amplitude events, we plotted example seismograms of low-magnitude events from Greece in Figs. 9. The signals are bandpass filtered with a lower cutoff

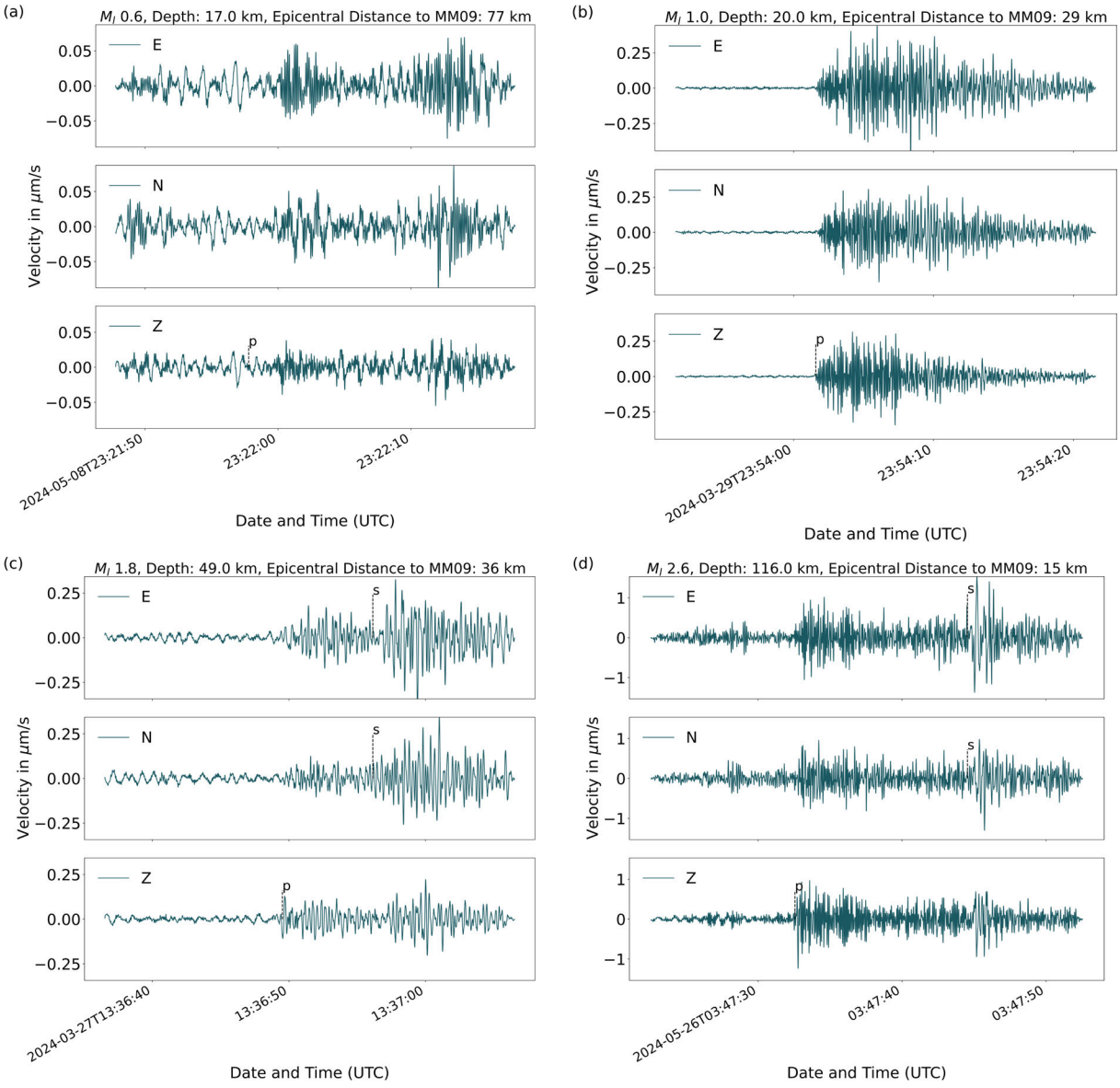

Figure 9. Three-component waveform recordings for four local earthquakes measured at station MM09. (a) The waveforms of the *ML* 0.6 earthquake on 8 June 2024, at a depth of 41 km and an epicentral distance of 77 km. (b) The waveforms of the *ML* 1.1 earthquake on 29 March 2024, at a depth of 20 km and an epicentral distance of 29 km. (c) The waveforms of the *ML* 1.8 earthquake on 27 March 2024, at a depth of 49 km and an epicentral distance of 36 km. (d) The waveforms of the *ML* 2.6 earthquake on 26 June 2024, at a depth of 116 km and an epicentral distance of 15 km.

The theoretical first arrivals are indicated, calculated using TauPy in ObsPy with the ak135 Earth model (Kennett et al., 1995). Note that the response function is removed. The recordings are bandpass filtered with a lower cutoff frequency of 1 Hz and an upper cutoff frequency of 15 Hz. Linear trends and the mean are subtracted.

frequency of 1 Hz and an upper cutoff frequency of 15 Hz. Figure 9a shows the three-component arrivals from an earthquake of local magnitude *ML* 0.6 that occurred east of Thiva, with an epicentral distance to MM09 of 77 km and a hypocentral depth of 17 km. Despite the large distance and small magnitude, the arrival of the wave is clearly visible. These preliminary indications suggest that the network meets the research goals (see Section 3), as events with magnitudes around ML ~ 0 may be detectable with a signal-to-noise ratio (SNR) greater than 3 within a 50 km radius, based on our calculated noise levels. In Figs. 9b recordings are displayed for an earthquake with local magnitude 1.0 at a hypocentral depth of 20 km and an epicentral distance of 29 km. The wavetrains are clearly visible with a strong first arrival onset. Figure 9c contains waveforms for an earthquake with a local magnitude *ML* of 1.8 that occurred at an epicentral distance of 39 km to MM09 at a hypocentral depth of 49 km. The P and S phases are clearly visible as well as the surface waves.

Since our study region also experiences intermediate-deep earthquakes resulting from the subduction processes, a possible tomography, anisotropy, or receiver function study would benefit from these ray paths as well. Figure 9d shows the arrivals from such a deep event (116 km depth) that occurred during the start of the recording period of the temporary deployment. This earthquake had a magnitude *ML* of 2.6 and an epicentral distance of 15 km to station MM09. The clear onsets of the P and S arrivals are marked and the SNR should allow to study the structure of the lithosphere and upper mantle above the hypocenter.

5. Discussion

Imaging ongoing magmatic and tectonic processes at depth require a well-planned seismic network design in order to measure microseismic events with sufficient SNR. In our case, the new occupation of four islands with seismic stations improved the regional station network (Fig. 5). This new network, MeMaX is centered on Methana Peninsula and its Quaternary volcanic field and it also well covers the adjacent submarine Pausanias Volcanic Field.

The analysis of seismic noise at the various sites demonstrates that the recording conditions are excellent. Based on our observations and noise level calculations, local events with magnitudes as low as ML ~ 0 are likely detectable within a 50 km radius. However, further data collection and analysis will be required to validate this hypothesis. This will allow us to map active faults (Fig. 2), e.g., using HypoDD (Waldhauser and Ellsworth, 2000), and to detect possible low frequency events which are known from other magmatic systems in the South Aegean Volcanic Arc, e.g., at the Santorini-Kolumbo magmatic system (Kolaitis et al., 2007). Therefore, MeMaX can contribute to the volcanic hazard assessment of the region. These results will then be supplemented with other ongoing studies in the Saronic Gulf with focus on Methana such as repeated drone flights with altitude measurements and drillings for tsunamigenic sediment layers at the coast.

The strategy to record temporarily with low-power instrumentation at remote sites worked well as can be seen by the noise level of −140 dB to −190 dB in the frequency range of 1-20 Hz for ground motion velocity (Figs. 6 and 7). The usage of solar panels with 20 W_{peak} and with a size of about 20 cm by 20 cm is enough to repower small rechargeable batteries (40 Ah in our case). Even if such solar panels cannot be installed in an optimal position to better conceal the station, additional independent tests conducted during winter times in Germany demonstrated that they still provide sufficient power for continuous recording. Such an installation is recommended for follow-up experiments to enable the monitoring of similar seismological and volcanic targets.

6. Conclusions

The temporary stations of the MeMaX network densify the existing permanent networks (HL and HA) to monitor microseismic activity associated with magmatic and tectonic processes in the Saronic Gulf, with a particular focus on the Methana and Pausanias magmatic systems. By using mobile short-period instruments with low power consumption, we can identify low-noise, remote sites that provide optimal conditions for achieving our research objectives. All temporary stations were installed on small cement foundations, firmly covered to the bedrock and with minimal sedimentary cover over the base limestone.

Initial quality control of the data suggests promising results for the upcoming recording periods, which allow high event detection rates, precise hypocentral earthquake locations, and improved local P- and S-wave velocity models. These advancements will enhance our understanding of the magmatic and tectonic activities in the Saronic

Gulf. The clear detection of onsets from low-magnitude earthquakes, as well as deep and distant events, indicates that the network is well-suited to achieve these research objectives.

Data and Resources. For completeness, we are providing the horizontal components of the probabilistic power spectral densities and the teleseismic events in the Appendix. The network and station information for network 1A, as well as for the permanent networks HA and HL, is available through EIDA. The data for the permanent stations was downloaded using ObsPy (Beyreuther et al., 2010) from the corresponding data center at NOA; however, it is only available with restricted access and is not publicly accessible (National Observatory of Athens, Institute of Geodynamics, Athens, 1975; University of Athens, 2008). Data from the MeMaX network 1A is restricted but is expected to become publicly available end of 2026 via EIDA web service of GEOFON (Föst et al., 2024). For data analysis, we used ObsPy, and all figures were created with either the Matplotlib library or the PyGMT library in Python (Hunter, 2007; Team, 2024) or the Generic Mapping Tools (Wessel et al., 2019). Colors were used from Crameri et al., (2024). The topography in figures is based on the ETOPO1 global relief model (Amante and Eakins, 2009). Information about teleseismic earthquakes was downloaded from USGS (https://earthquake.usgs.gov/earthquakes). The event catalogs for local seismicity were downloaded from the National Observatory of Athens and are publicly available at (https://www.gein.noa.gr/en/services-products/earthquake-catalogs/).

Acknowledgements. J.-P.F. would like to thank Moritz Lang, a fellow PhD candidate and collaborator on this project. Together, we explored this new topic, working closely to collect data and deepen our understanding of the region. The authors also wish to thank Moritz Lang, Charlotte Petrikowski, Kyriakos Kontakos, and Ioannis Fountoulakis for their assistance in fieldwork. The temporary recording instruments were provided by the Geophysical Instrument Pool of GFZ Potsdam under Grant (GIPP202407). This study was supported by grant no. FKZ: 03F0952C of the German Federal Ministry of Education and Research (BMBF) as part of the DAM mission 'mareXtreme', project MULTI-MAREX.

References

Aki, K. and R. Koyanagi (1981). Deep volcanic tremor and magma ascent mechanism under Kilauea, Hawaii, J. Geophys. Res.-Sol. Ea., 86, B8, 7095-7109, doi:10.1029/JB086iB08p07095.

Aki, K. and P. G. Richards (1980). Quantitative Seismology, University Science Books, 726.

Amante, C. and B. W. Eakins, n.d., ETOPO1 1 Arc-Minute Global Relief Model: NOAA Technical Memorandum NESDIS NGDC-24, v. National Geophysical Data Center, Boulder, Colorado, 19.

Antoniou, V., L. Ragia, P. Nomikou, P. Bardouli et al. (2018). Creating a Story Map Using Geographic Information Systems to Explore Geomorphology and History of Methana Peninsula, ISPRS Int. J. of Geo-Info., 7, 12, 484, doi:10.3390/ijgi7120484.

Batte, A. G., A. Schumann and E. M. Twesigomwe (2021). Seismic anisotropy accrued by seven unusually deep local earthquakes (between 50 and 60 km) in the Albertine Rift: implications of asthenospheric melt upwelling, J. Seismol., 25, 3, 921-936, doi:10.1007/s10950-021-10007-2.

Beyreuther, M., R. Barsch, L. Krischer, T. Megies et al. (2010). ObsPy: A Python Toolbox for Seismology, Seismol. Res. Letters, v. 81, no. 3, p. 530-533, doi:10.1785/gssrl.81.3.530.

Clarke, P. J., R. R. Davies, P. C. England, B. Parsons et al. (1998). Crustal strain in central Greece from repeated GPS measurements in the interval 1989-1997, Geophys. J. Int., 135, 1,195-214, doi:10.1046/j.1365-246X.1998.00633.x.

Crameri, F., G. E. Shephard and P. J. Heron (2024). Choosing Suitable Color Palettes for Accessible and Accurate Science Figures, Current Protocols, 4, 8, e1126, doi:10.1002/cpz1.1126.

D'Alessandro, W., L. Brusca, K. Kyriakopoulos, G. Michas et al. (2008). Methana, the westernmost active volcanic system of the south Aegean arc (Greece): Insight from fluids geochemistry, J. Volcanol. Geoth. Res., 178, 4, 818-828, doi:10.1016/j.jvolgeores.2008.09.014.

Dietrich, V., I. Mercolli and R. Oberhänsli (1988). Dazite, High-Alumina-Basalte und Andesite als Produkte amphiboldominierter Differentation (Aegina und Methan, Ägäischer Inselbogen), Schweiz. Mineral. Petrogr. Mitt., 68, 21-39.

Dotsika, E., D. Poutoukis and B. Raco (2010). Fluid geochemistry of the Methana Peninsula and Loutraki geothermal area, Greece, J. Geochem. Explor.,104, 3, 97-104, doi:10.1016/j.gexplo.2010.01.001.

Drakatos, G., V. Karastathis, J. Makris, J. Papoulia et al. (2005). 3D crustal structure in the neotectonic basin of the Gulf of Saronikos (Greece), Tectonophys., 400, 1-4, 55-65, doi:10.1016/j.tecto.2005.02.004.

Eberhart-Phillips, D. and A. J. Michael (1993). Three-dimensional velocity structure, seismicity, and fault structure in the Parkfield Region, central California, J. Geophys. Res.-Sol. Ea., 98, B9, 15737-15758, doi:10.1029/93JB01029.

Elburg, M. A., I. Smet, P. Van Den Haute, F. Vanhaecke et al. (2018). Extreme isotopic variation documents extensional tectonics in arc magmas from Methana, Greece, Lithos, 318-319, 386-398, doi:10.1016/j.lithos.2018.08.029.

Evangelidis, C. P., N. Triantafyllis, M. Samios, K. Boukouras et al. (2021). Seismic Waveform Data from Greece and Cyprus: Integration, Archival, and Open Access, Seismol. Res. Lett., 92, 3, 1672-1684, doi:10.1785/0220200408.

Föst, J.-P., N. Richter and J. Ritter (2024). Methana Magmatic Observational Experiment (MeMaX), GFZ Data Services, doi:10.14470/6N477343.

Foutrakis, P. M. and G. Anastasakis (2018a). Bathy-morphological setting of the Submarine Pausanias Volcanic Field, South Aegean Active Volcanic Arc, J. Maps, 14, 2, 341-347, doi:10.1080/17445647.2018.1473816.

Foutrakis, P. M. and G. Anastasakis (2018b). The active submarine NW termination of the South Aegean Active Volcanic Arc: The Submarine Pausanias Volcanic Field, J. Volcanol. Geoth. Res., 357, doi:10.1016/j.jvolgeores.2018.05.008.

Foutrakis, P. M. and G. Anastasakis (2020). Quaternary continental shelf basins of Saronikos Gulf, Aegean Sea, Geo-Marine Lett., 40, 5, 629-647, doi:10.1007/s00367-020-00653-9.

Fytikas, M., F. Innocenti, P. Manetti, A. Peccerillo et al. (1984). Tertiary to Quaternary evolution of volcanism in the Aegean region: The Geological Evolution of the Eastern Mediterranean, in Geological Society Special Publication The Geological Evolution of the Eastern Mediterranean, The Geological Society Publishing House, 687-699.

Gatsios, T., F. Cigna, D. Tapete, V. Sakkas et al. (2020a). Copernicus Sentinel-1 MT-InSAR, GNSS and Seismic Monitoring of Deformation Patterns and Trends at the Methana Volcano, Greece, Appl. Sci., 10, 18, 6445, doi:10.3390/app10186445.

Gatsios, T., F. Cigna, D. Tapete, V. Sakkas et al. (2020b). Investigating 2015-2019 deformation patterns at the Methana volcano in Greece using Sentinel-1 MT-InSAR, GNSS/GPS and seismic data, in Proceedings of The 3rd International Electronic Conference on Geosciences, Sciforum.net, MDPI, 8547, doi:10.3390/IECG2020-08547.

Grove, T., N. Chatterjee, S. Parman and E. Medard (2006). The influence of H2O on mantle wedge melting, Earth Planet. Sci. Lett., 249, 1-2, 74-89, doi:10.1016/j.epsl.2006.06.043.

Haslinger, F. and E. Kissling (2001). Investigating effects of 3-D ray tracing methods in local earthquake tomography, Phys. Earth Planet. Int., 123, 2-4, 103-114, doi:10.1016/S0031-9201(00)00204-1.

Hatzfeld, D., G. Pedotti, P. Hatzidimitriou, D. Panagiotopoulos et al. (1989). The Hellenic subduction beneath the Peloponnesus: first results of a microearthquake study, Earth Planet. Sci. Lett., 93, 2, 283-291, doi:10.1016/0012-821X(89)90076-9.

Hensch, M., T. Dahm, J. Ritter, S. Heimann et al. (2019). Deep low-frequency earthquakes reveal ongoing magmatic recharge beneath Laacher See Volcano (Eifel, Germany), Geophys. J. Int., 216, 3, 2025-2036, doi:10.1093/gji/ggy532.

Hunter, J. D. (2007). Matplotlib: A 2D Graphics Environment, Computing in Science & Engineering, 9, 3, 90-95, doi:10.1109/MCSE.2007.55.

Jolivet, L., C. Faccenna, B. Huet, L. Labrousse et al. (2013). Aegean tectonics: Strain localisation, slab tearing and trench retreat, Tectonophys., 597-598, 1-33, doi:10.1016/j.tecto.2012.06.011.

Karagianni, E. E., C. B. Papazachos, D. G. Panagiotopoulos, P. Suhadolc et al. (2004). Shear velocity structure in the Aegean area obtained by inversion of Rayleigh waves: Shear velocity structure in the Aegean area, Geophys. J. Int., 160, 1, 127-143, doi:10.1111/j.1365-246X.2005.02354.x.

Kennett, B. L. N., E. R. Engdahl and R. Buland (1995). Constraints on seismic velocities in the Earth from traveltimes, Geophys. J. Int., 122, 1, 108-124, doi:10.1111/j.1365-246X.1995.tb03540.x.

Kissling, E., W. L. Ellsworth, D. Eberhart-Phillips and U. Kradolfer (1994). Initial reference models in local earthquake tomography, J. Geophys. Res.-Sol. Earth, 99, B10, 19635-19646, doi:10.1029/93JB03138.

Kissling, E., U. Kradolfer and H. Maurer (1995). Program VELEST user ‘s guide – Short Introduction, Institute of Geophysics, ETH Zürich. https://seg.ethz.ch/software/velest.html, Accessed 26 November 2024.

Kolaiti, E. and N. D. Mourtzas (2016). Upper Holocene sea level changes in the West Saronic Gulf, Greece, Quaternary Int., 401, 71-90, doi:10.1016/j.quaint.2015.06.024.

Kolaitis, A., P. Papadimiriou, I. Kassaras and K. Makropoulos (2007). Seismic observations with broadband instruments at Santorini volcano, Bull. Geolog. Soc. of Greece, 40, 3, 1150-1161, doi:10.12681/bgsg.16844.

Kusky, T. M., E. Bozkurt, J. Meng and L. Wang (2023). Twin Earthquakes Devastate Southeast Türkiye and Syria: First Report from the Epicenters, J. of Earth Sci., 34, 2, 291-296, doi:10.1007/s12583-023-1317-5.

Le Pichon, X. and J. Angelier (1979). The Hellenic Arc and Trench System: a key to the neotectonic evolution of the Eastern Mediterranean Area, Tectonophys., 60, 1-42, doi:10.1016/0040-1951(79)90131-8.

Le Pichon, X., J. Angelier, M. F. Osmaston, L. Stegena et al. (1997). The Aegean Sea, Philosophical Transactions of the Royal Society of London. Series A, Math. Phys. Sci., 300, 1454, 357-372, doi:10.1098/rsta.1981.0069.

Makris, J., J. Papoulia and G. Drakatos (2004). Tectonic Deformation and Microseismicity of the Saronikos Gulf, Greece, Bull. Seismol. Soc. Am., 94, 3, 920-929, doi:10.1785/0120020209.

Mani, L., A. Tzachor and P. Cole (2021). Global catastrophic risk from lower magnitude volcanic eruptions, Nature Commun., 12, 1, 4756, doi:10.1038/s41467-021-25021-8.

McClusky, S., S. Balassanian, A. Barka, C. Demir et al. (2000). Global Positioning System constraints on plate kinematics and dynamics in the eastern Mediterranean and Caucasus, J. Geophys. Res.-Sol. Earth, 105, B3, 5695-5719, doi:10.1029/1999JB900351.

Münchmeyer, J., J. Woollam, A. Rietbrock, F. Tilmann et al. (2022). Which Picker Fits My Data? A Quantitative Evaluation of Deep Learning Based Seismic Pickers, J. Geophys. Res.-Sol. Earth,127,1, e2021JB023499, doi:10.1029/2021JB023499.

National Observatory of Athens, Institute of Geodynamics, Athens (1975). National Observatory of Athens Seismic Network, International Federation of Digital Seismograph Networks, doi:10.7914/SN/HL.

Nomikou, P., D. Papanikolaou, M. Alexandri, D. Sakellariou et al. (2013). Submarine volcanoes along the Aegean volcanic arc, Tectonophys., 597-598,123-146, doi:10.1016/j.tecto.2012.10.001.

Pallister, J. and S. R. McNutt (2015). Synthesis of Volcano Monitoring, in The Encyclopedia of Volcanoes, Elsevier, 1151-1171, doi:10.1016/B978-0-12-385938-9.00066-3.

Papageorgiou, E. (2010). Crustal Movements along the NW Hellenic Volcanic Arc from DGPS Measurements, 1, Bull. Geolog. Soc. of Greece, 43, 1, 331-343, doi:10.12681/bgsg.11185.

Papanikolaou, D. I. (2021). The Geology of Greece, Cham, Springer International Publishing, Regional Geology Reviews, doi:10.1007/978-3-030-60731-9.

Papanikolaou, D., V. Lykousis, G. Chronis and P. Pavlakis (1988). A comparative study of neotectonic basins across the Hellenic arc: the Messiniakos, Argolikos, Saronikos and Southern Evoikos Gulfs, Basin Res., 1, 3, 167-176, doi:10.1111/j.1365-2117.1988.tb00013.x.

Papazachos, C. (2019). Deep Structure and Active Tectonics of the South Aegean Volcanic Arc, Elements, 15, 153-158, doi:10.2138/gselements.15.3.153.

Papazachos, B. C. and P. E. Comninakis (1971). Geophysical and tectonic features of the Aegean Arc, J. Geophys. Res., 76, 35, 8517-8533, doi:10.1029/JB076i035p08517.

Pe-Piper, G. and D. J. W. Piper (2013). The effect of changing regional tectonics on an arc volcano: Methana, Greece, J. Volcanol. Geoth. Res., 260, 146-163, doi:10.1016/j.jvolgeores.2013.05.011.

Pe-Piper, G. and D. J. W. Piper (2002). The igneous rocks of Greece: The Anatomy of an Orogen, Geological Magazine, doi:10.1017/S0016756803218021.

Pe-Piper, G. and D. Piper (2005). The South Aegean active volcanic arc: Relationships between magmatism and tectonics, Dev. Volcanol., 7, 113-133, doi:10.1016/S1871-644X(05)80034-8.

Peterson, J. R. (1993). Observations and modeling of seismic background noise, 93-322: U.S. Geological Survey, doi:10.3133/ofr93322.

Ritter, J. R. R., M. Koushesh, B. Schmidt, J.-P. Föst et al. (2024). Seismological Monitoring of Magmatic and Tectonic Earthquakes in the East Eifel Volcanic Field, Germany, J. Seismol., doi:10.1007/s10950-024-10257-w.

Rout, S. S., M. Blum-Oeste and G. Wörner (2021). Long-Term Temperature Cycling in a Shallow Magma Reservoir, Insights from Sanidine Megacrysts at Taápaca Volcano, Central Andes, J. Petrol., 62, 9, egab010, doi:10.1093/petrology/egab010.

Sachpazi, M., M. Laigle, M. Charalampakis, J. Diaz et al. (2016). Segmented Hellenic slab rollback driving Aegean deformation and seismicity, Geophys. Res. Lett., 43, 2, 651-658, doi:10.1002/2015GL066818.

Scherbaum, F. (2001). Of Poles and Zeros, Dordrecht, Springer Netherlands, Modern Approaches in Geophysics, doi:10.1007/978-1-4020-6861-4.

Schoenhofen, M. V., K. M. Haase, C. Beier, D. Woelki et al. (2020). Chemical Evolution of Calc-alkaline Magmas during the Ascent through Continental Crust: Constraints from Methana, Aegean Arc, J. of Petrol., 61, 3, egaa036, doi:10.1093/petrology/egaa036.

Skourtsos, E. and H. Kranis (2009). Structure and evolution of the western Corinth Rift, through new field data from the Northern Peloponnesus, Geological Society, London, Special Pub., 321, 1, 119-138, doi:10.1144/SP321.6.

Stefatos, A., G. Papatheodorou, G. Ferentinos, M. Leeder et al. (2002). Seismic reflection imaging of active offshore faults in the Gulf of Corinth: their seismotectonic significance, Basin Res., 14, 4, 487-502, doi:10.1046/j.1365-2117.2002.00176.x.

Suckale, J., S. Rondenay, M. Sachpazi, M. Charalampakis et al. (2009). High-resolution seismic imaging of the western Hellenic subduction zone using teleseismic scattered waves, Geophys. J. Int., 178, 2, 775-791, doi:10.1111/j.1365-246X.2009.04170.x.

Sun, H., Z. E. Ross, W. Zhu and K. Azizzadenesheli (2023). Phase Neural Operator for Multi-Station Picking of Seismic Arrivals, Geophys. Res. Lett., 50, 24, e2023GL106434, doi:10.1029/2023GL106434.

Team, T. M. D. (2024). Matplotlib: Visualization with Python, Zenodo, doi:10.5281/zenodo.13308876.

Thurber, C. H. (1983). Earthquake locations and three-dimensional crustal structure in the Coyote Lake Area, central California, J. Geophys. Res.-Sol. Earth, 88, B10, 8226-8236, doi:10.1029/JB088iB10p08226.

Tzanis, A., A. Efstathiou, S. Chailas, E. Lagios et al. (2020). The Methana Volcano – Geothermal Resource, Greece, and its relationship to regional tectonics, J. Volcanol. Geoth. Res., 404, 107035, doi:10.1016/j.jvolgeores.2020.107035.

Tzanis, A., A. Efstathiou, S. Chailas and M. Stamatakis (2018). Evidence of recent plutonic magmatism beneath Northeast Peloponnesus (Greece) and its relationship to regional tectonics, Geophys. J. Int., 212, 3, 1600-1626, doi:10.1093/gji/ggx486.

University of Athens (2008). Hellenic Seismological Network, University of Athens, Seismological Laboratory, International Federation of Digital Seismograph Networks, doi:10.7914/SN/HA.

Vougioukalakis, G. E. and M. Fytikas (2005). Volcanic hazards in the Aegean area, relative risk evaluation, monitoring and present state of the active volcanic centers, in Michael Fytikas and Georges E. Vougioukalakis, eds., Developments in Volcanology, Elsevier, The South Aegean Active Volcanic Arc, 161-183, doi:10.1016/S1871-644X(05)80037-3.

Waldhauser, F. and W. L. Ellsworth (2000). A Double-Difference Earthquake Location Algorithm: Method and Application to the Northern Hayward Fault, California, Bull. Seismol. Soc. Am., 90, 6, 1353-1368, doi:10.1785/0120000006.

Wessel, P., J. F. Luis, L. Uieda, R. Scharroo et al. (2019). The Generic Mapping Tools Version 6, Geochem., Geophys., Geosys., 20, 11, 5556-5564, doi:10.1029/2019GC008515.

White, R. A. and W. A. McCausland (2019). A process-based model of pre-eruption seismicity patterns and its use for eruption forecasting at dormant stratovolcanoes, J. Volcanol. Geoth. Res., 382, 267-297, doi:10.1016/j.jvolgeores.2019.03.004.

Woelki, D., K. M. Haase, M. V. Schoenhofen, C. Beier et al. (2018). Evidence for melting of subducting carbonate-rich sediments in the western Aegean Arc, Chemical Geology, 483, 463-473, doi:10.1016/j.chemgeo.2018.03.014.

Woollam, J. et al. (2022). SeisBench – A Toolbox for Machine Learning in Seismology, Seismol. Res. Lett., 93, 3, 1695-1709, doi:10.1785/0220210324.

***CORRESPONDING AUTHOR: Jan-Phillip FÖST**,
RWTH Aachen University, Teaching and Research Area Neotectonics and Natural Hazards, Aachen, Germany
e-mail: jp.foest@nug.rwth-aachen.de